

1 **Measurement Report: Wintertime new particle formation in the rural area of North**
2 **China Plain: influencing factors and possible formation mechanism**

3
4
5 **Juan Hong^{1,2†*}, Min Tang^{1,2†}, Qiaoqiao Wang^{1,2*}, Nan Ma^{1,2}, Shaowen Zhu^{1,2}, Shaobin**
6 **Zhang^{1,2}, Xihao Pan^{1,2}, Linhong Xie^{1,2}, Guo Li³, Uwe Kuhn³, Chao Yan⁴, Jiangchuan**
7 **Tao^{1,2}, Ye Kuang^{1,2}, Yao He^{1,2}, Wanyun Xu⁵, Runlong Cai⁶, Yaqing Zhou^{1,2}, Zhibin**
8 **Wang⁷, Guangsheng Zhou⁵, Bin Yuan¹, Yafang Cheng³, Hang Su³**

9
10 ¹Institute for Environmental and Climate Research, Jinan University, Guangzhou, Guangdong
11 511443, China

12 ²Guangdong-Hongkong-Macau Joint Laboratory of Collaborative Innovation for Environmental
13 Quality, Guangzhou, China

14 ³Multiphase Chemistry Department, Max Planck Institute for Chemistry, Mainz 55128, Germany

15 ⁴School of Atmospheric Sciences, Joint International Research Laboratory of Atmospheric and
16 Earth System Sciences, Nanjing University, Nanjing, China

17 ⁵Hebei Gucheng, Agrometeorology, National Observation and Research Station, Chinese Academy
18 of Meteorological Sciences, Beijing, 100081, China

19 ⁶Institute for Atmospheric and Earth System Research/Physics, Faculty of Science, University of
20 Helsinki, Helsinki, FI00014, Finland

21 ⁷College of Environmental and Resource Sciences, Zhejiang University, Zhejiang Provincial Key
22 Laboratory of Organic Pollution Process and Control, Hangzhou 310058, China

23 [†]These authors contributed equally to this work.

24 *Correspondence: Qiaoqiao Wang (qwang@jnu.edu.cn) and Juan Hong
25 (juanhong0108@jnu.edu.cn)

26
27 **Abstract:**

28 The high concentration of fine particles as well as gaseous pollutants makes
29 polluted areas, such as the urban setting of North China Plain (NCP) of China, a
30 different environment for NPF compared to many clean regions. Such conditions also
31 hold for other polluted environments in this region, for instance, the rural area of
32 NCP, yet the underlying mechanisms for NPF remain less understood owing to the
33 limited observations of particles in the sub-3nm range. Comprehensive
34 measurements, particularly covering the particle number size distribution down to
35 1.3 nm, were conducted at a rural background site of Gucheng (GC) in the North
36 China Plain (NCP) from 12 November to 24 December in 2018. Five NPF events
37 during the 39 effective days of measurements for the campaign were identified, with

38 the mean particle nucleation rate ($J_{1.3}$) and growth rate ($GR_{1.3-2.4}$) were $22.0 \text{ cm}^{-3}\cdot\text{s}^{-1}$
39 and $3.9 \text{ nm}\cdot\text{h}^{-1}$, respectively. During these five days, NPF concurrently occurred at an
40 urban site in Beijing. Sharing similar sources and transport paths of air masses
41 arriving at our site to that of urban Beijing, we hypothesis that NPF events during
42 these days in this region might be a regional phenomenon. The simultaneous
43 occurrence of NPF in both places implies that H_2SO_4 -amine nucleation, concluded for
44 urban Beijing there, could probably be the dominating mechanism for NPF at our
45 rural site. The higher concentration of sulfuric acid during many non-event days
46 compared to that of event days indicates that the content of sulfuric acid may not
47 necessarily lead to NPF events under current atmosphere. Only when the
48 condensation sink or coagulation sink was significantly lowered, atmospheric NPF
49 occurred, implying that CS or CoagS are the dominating factor controlling the
50 occurrence of NPF for present rural environment of NCP, being quite similar to the
51 feature at urban Beijing.

52

53 **Keywords:** new particle formation, particle number size distribution, condensational
54 sink, nucleation mechanism.

55 **1. Introduction**

56 Atmospheric new particle formation (NPF) is a major source of the global
57 particles in terms of number concentration and size distribution (Kulmala et al., 2004)
58 and is considered to contribute up to half of the global cloud condensation nuclei
59 (CCN) budget in the lower troposphere (Spracklen et al., 2006; Dunne et al., 2016). In
60 general, NPF consists of two consecutive processes: a) the formation or nucleation of
61 molecular clusters by low-volatile gaseous substances, and b) their subsequent
62 growth to detectable sizes or even larger, at which these particles may act as CCN or
63 contribute to the particle mass concentration (Kulmala et al., 2000; Zhang et al.,
64 2012).

65 Numerous laboratory measurements and field studies have shown that sulfuric
66 acid molecules (H_2SO_4) are one of the key precursors to form molecular clusters for
67 nucleation (Nieminen et al., 2010; Sipilä et al., 2010; Kirkby et al., 2011; Riccobono et
68 al., 2014; Stolzenburg et al., 2020). However, these H_2SO_4 clusters relevant to
69 atmospheric nucleation are typically quite small, i.e., with diameters below 1.5 nm,
70 at which the detection efficiency of traditional instruments specific for NPF was
71 usually unsatisfactory (Kulmala et al., 2013). This had led to large uncertainties in the
72 measured formation rate of newly formed particles and thus required precise
73 measurements of these clusters or particles down to sub-3 nm. Upon recently,
74 progress such as the use of a particle size magnifier (PSM) (Vanhanen et al., 2011;
75 Xiao et al., 2015), a neutral cluster and air ion spectrometer (NAIS) (Mirme and
76 Mirme, 2013) and a chemical ionization atmospheric pressure interface time-of-flight
77 mass spectrometer (CI-API-TOF) (Jokinen et al., 2012) make it possible to directly
78 measure the number concentration of clusters in the 1-3 nm size range. Benefit from
79 these novel techniques, observations have found that the growth of H_2SO_4 clusters
80 would be significantly promoted after stabilized by other precursors like amines,
81 ammonia or iodine species (Berndt et al., 2010; Kirkby et al., 2011; Almeida et al.,
82 2013; Riccobono et al., 2014; Kürten et al., 2016; Sipilä et al., 2010). Furthermore,

83 oxidation products from volatile organic compounds, for instance, highly oxidized
84 organic compounds, were suggested to be important contributors to atmospheric
85 nucleation (Ehn et al., 2014; Bianchi et al., 2016; Kirkby et al., 2016; Tröstl et al.,
86 2016).

87 The North China Plain (NCP) of China, has been suffering heavily from the highly
88 complex air pollution since decades (Ma et al., 2016; Shen et al., 2018; Zhang et al.,
89 2020), owing to the high emissions or formation of different pollutants such as SO₂,
90 NH₃, VOCs as well as fine particles from various sources (Guo et al., 2014; Zhang et al.,
91 2015). Due to the high concentration of pre-existing particles, previous studies
92 considered that in the NCP, less NPF would occur as the newly-formed particles
93 would be scavenged much faster before growing. By contrast, atmospheric NPF was
94 still frequently observed in this region (Chu et al., 2019; Deng et al., 2020; Cai et al.,
95 2021), being more often than theoretically predicted (Kulmala et al., 2014), indicating
96 that the underlying mechanisms for NPF in this area might be different, that those
97 mechanism previously found for other environments might not be completely
98 applicable. The higher concentration of these gaseous precursors makes this region
99 an unique condition for NPF compared to relatively clean environments (Kulmama et
100 al., 2016; Yu et al., 2017; Wang et al., 2017), further supporting the hypothesis of
101 different formation mechanisms and thereby distinct features of NPF events in this
102 region. These doubts concerning NPF in the NCP, however, still remain to be
103 elucidated due to limitations of comprehensive measurements, particularly for rural
104 areas of the NCP, where observations regarding NPF was even more rare.

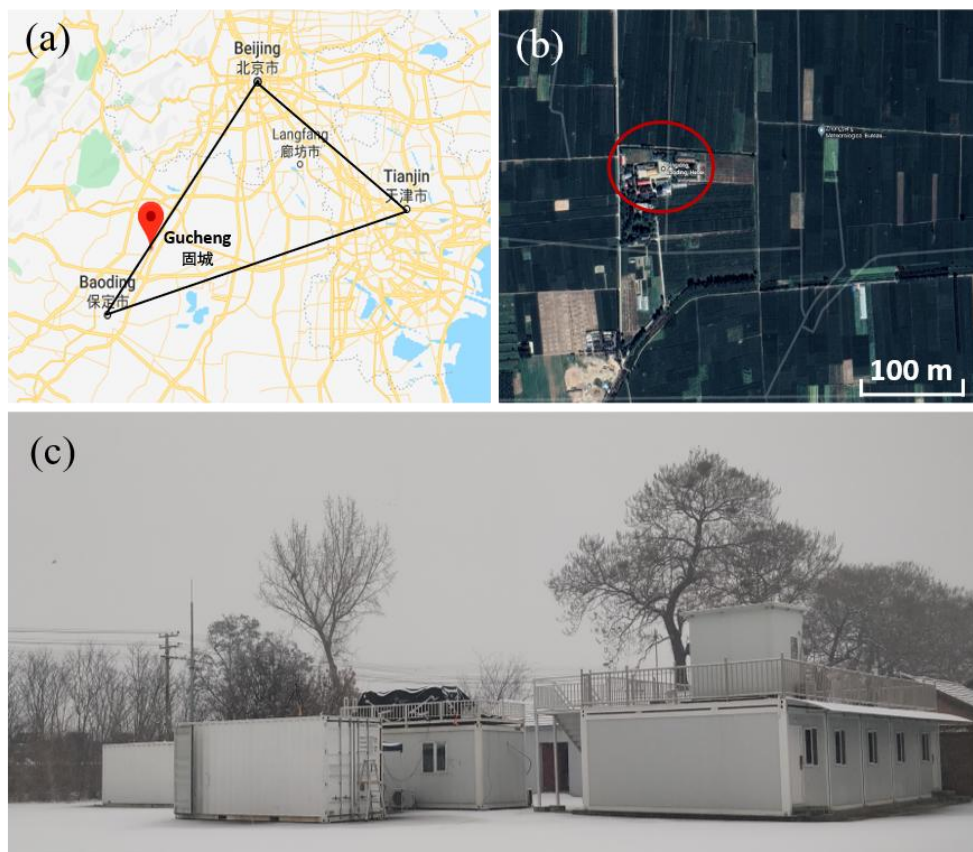
105 In addition, with respect to those existing studies concerning NPF in the NCP,
106 they mainly focused on the measurements of particles beyond 3 nm. Without
107 applicable instruments, observations of new particles down to sub-3nm was still
108 quite limited (Fang et al., (2020); Zhou et al., (2020)), causing large uncertainties in
109 the measured characteristics of NPF for current region. To fill the gap of
110 measurements of particles or clusters in the size range of 1-3 nm and further
111 advance our understanding of NPF in this region, particularly in the rural area of NCP,
112 we conducted a comprehensive measurement campaign at a rural background site in

113 the NCP during 12 November to 24 December, 2018. By obtaining the particle
114 number size distribution over a wide diameter range (1.3 nm - 10 μ m), we aimed to
115 investigate the characteristics of NPF events at the rural site in NCP during
116 wintertime, find out which factors govern the occurring of NPF compared to other
117 regions of NCP such as the urban areas and explore the potential mechanisms for
118 NPF in this area.

119 **2. Experiment**

120 **2.1. Field measurements site**

121 The measurements were conducted at Gucheng (GC) site ($39^{\circ}09'01.1''\text{N}$
122 $115^{\circ}44'02.6''\text{E}$), situated at an Ecological and Agricultural Meteorology Station
123 ($39^{\circ}09' \text{ N}$, $115^{\circ}44' \text{ E}$) of the Chinese Academy of Meteorological Sciences from 12
124 November to 24 December in 2018. The station is located in Dingxing county,
125 Baoding city, Hebei Province, China, as seen in Fig.1 and surrounded by agricultural
126 fields and sporadic villages. Being far from the urban and industrial emission areas,
127 this site can be treated as a representative regional site in the northern part of NCP.
128 More details about this site can be found in Lin et al. (2009) and Shen et al. (2018).



129
130 Figure 1. The upper panel shows the geographical location of the site (red dot and circled, ©
131 Google Maps), where our field measurements were carried out. The lower panel shows the
132 measurement containers, where the sampling instruments were set up.

133 **2.2. Measurements**

134 **2.2.1. Particle Number Size Distribution (PNSD) measurement**

135 The aerosol sampling inlet was located on the rooftop of a measurement
136 container, where room temperature was maintained at 22 °C (Fig1. c). The aerosol
137 was sampled via a low-flow PM₁₀ cyclone inlet, passed through a Nafion dryer, and
138 directed to different instruments through stainless steel or conductive black tubings
139 using an isokinetic flow splitter. The particle number size distribution of aerosol
140 particles with diameters from 10 nm to 10000 nm was measured by using a scanning
141 mobility particle sizer (SMPS, model TSI 3938) and an Aerodynamic Particle Size
142 Spectrometer (APS, model TSI 3321) at a time resolution of around 5 minutes. The
143 SMPS consisted of an electrostatic classifier (model TSI 3080) and a condensation
144 particle counter (CPC, model TSI 3772).

145 **2.2.2. Sub-3nm Particle Number Concentration measurement**

146 Sub-3nm particles were measured with an Airmodus nano Condensation
147 Nucleus Counter system (nCNC, model A11), consisting of a Particle Size Magnifier
148 (PSM, model A10) and a butanol condensation particle counter (CPC, model A20)
149 (Vanhanen et al., 2011). The Airmodus PSM uses diethylene glycol as the working
150 fluid to activate and grow nano-sized particles. Specifically, the PSM was operated
151 under the scanning mode that the diethylene glycol flow was varied between 0.1 to
152 1.3 L·min⁻¹. Thus, the number size distribution of five different size bins, i.e., 1.3-1.4,
153 1.4-1.6, 1.6-1.9, 1.9-2.4, and 2.4-3.7 nm was obtained. Owing to the data quality,
154 only the former four size bins data were used in this study. During this campaign, the
155 duration of each scan was completed within around 240 s.

156 **2.2.3. Pollutant gases, PM_{2.5} and meteorological parameters measurement**

157 Concentration of trace gases, including SO₂, O₃, CO and NO_x, was measured
158 continuously during this campaign using different Thermo Fisher Analysers (model

159 43i-TLE, 49i, 48i, and 42i), respectively, at a time resolution of 1 minute. The
160 concentration of oxygenated volatile organic compounds (OVOCs) was measured
161 with an iodide-adduct long time-of-flight chemical ionization mass spectrometer
162 (I-CIMS, Aerodyne, US) at a time resolution of 10-30 s for current study.

163 In addition, ambient meteorological conditions, such as wind speed, wind
164 direction, temperature, relative humidity and solar radiation, were also regularly
165 measured in another building, which is located about 20 meters to the southwest of
166 the container, at the same observational site.

167 Furthermore, in order to investigate the influence of the origins and transport
168 paths of air parcels to the local atmospheric compositions during NPF events, 72-h
169 back trajectories of air masses arriving at 100 m above ground level at our GC site
170 were analyzed using the HYbrid Single-Particle Lagrangian Integrated Trajectory
171 (HYSPLIT) model for the classified event days.

172 **2.3. Data processing**

173 **2.3.1. Formation Rate (J_{D_p}) and Growth Rate (GR)**

174 J_{D_p} defines the formation rate of atmospheric particles at a certain diameter (D_p)
175 and can be calculated according to Kulmala et al. (2012) as:

$$J_{D_p} = \frac{dN_{\Delta D_p}}{dt} + CoagS_{\Delta D_p} \times N_{\Delta D_p} + \frac{1}{\Delta D_p} GR_{\Delta D_p} \times N_{\Delta D_p}$$

176 where N is the particle number concentration between the diameter dp_2 and dp_1
177 (denotes as ΔD_p), $CoagS$ is the coagulation sink of particles, GR is the particle
178 growth rate out of the selected size bin.

179 In our study, we used two independent methods to calculate GR. One is the
180 maximum concentration method (Kulmala et al., 2012), being mainly for the PSM
181 data. The other is based on the variation in geometric mean diameters of particle
182 number size distribution, which is derived by fitting the PNSD into 2 or 3 log-normal
183 modes using an automatic algorithm (DO-FIT model) (Hussein et al., 2005), mainly for
184 SMPS data.

$$GR = \frac{ddp}{dt} = \frac{\Delta dp}{\Delta t} = \frac{dp_2 - dp_1}{t_2 - t_1}$$

185 where dp_1 and dp_2 were particle diameters at time t_1 and t_2 , respectively.

186 2.3.2. Condensation Sink (CS) and Coagulation Sink (CoagS)

187 CS describes how fast the low-volatility molecules condense onto pre-existing
188 aerosols and can be expressed as (Kulmala et al., 2012):

$$CS = 2\pi D \int_0^{dp_{max}} \beta_{m,dp} dp N_{dp} ddp = 2\pi D \sum_{dp} \beta_{m,dp} dp N_{dp}$$

189 where D is the diffusion coefficient of the condensing vapor, which is usually referred
190 to sulfuric acid and $\beta_{m,dp}$ is the mass flux transition correction factor.

191 CoagS represents how fast the freshly formed particles are lost to pre-existing
192 particles through coagulation and can be calculated as :

$$CoagS_{dp} = \int K(dp, dp') n(dp) ddp' \cong \sum_{dp'=dp}^{dp'=max} K(dp, dp') N_{dp'}$$

193 where, $K(dp, dp')$ is the collision efficiency between particles at the diameter from
194 dp to dp' .

195 2.3.3. Sulfuric Acid proxy (SA proxy)

196 SA was considered as one of the key precursors responsible for particle
197 nucleation in the atmosphere. However, no direct measurement for the
198 concentration of SA was available in current study. We therefore used a proxy
199 variable to substitute the concentration of SA, as SA is mainly produced by the
200 oxidation of SO_2 by OH radicals, which can be approximated by the UV-B intensity
201 (Petäjä et al., 2009). Thus, the proxy concentration of SA can be calculated by Lu et al.
202 (2019):

$$203 SA \text{ proxy} = 0.0013 \cdot UVB^{0.13} \cdot [SO_2]^{0.40} \cdot CS^{-0.17} \cdot ([O_3]^{0.44} + [NO_x]^{0.41})$$

204 **2.3.4. Classification of NPF event**

205 Days of NPF events was classified according to the method proposed by Dal
206 Maso et al. (2005) and Kulmala et al. (2012), in which (a) a burst in the concentration
207 of sub-3 nm particles or clusters was observed and (b) these particles had a
208 continuous growth over a time span of hours (e.g., usually more than ten hours). If
209 no clear growth of these newly formed particles (sub-3 nm particles) can be
210 identified, the day was classified as an undefined day. The day without both the
211 burst of sub-3 nm particles and their subsequent growth was considered as a
212 non-event day.

213 **2.3.5. Indicator for the occurrence of NPF**

214 Previously, McMurry et al. (2005) proposed a dimensionless criterion, L , to
215 predict the occurrence of NPF events in the atmosphere. After being validated in
216 diverse atmospheric environments (Kuang et al., 2010; Cai et al., 2017), L has been
217 used to investigate the governing factors for NPF events under typical atmospheric
218 conditions. Upon recently, Cai et al. (2021a) proposed a new indicator, I , on the basis
219 of L , which only considered H_2SO_4 to drive the growth. The new indicator was
220 calculated by further taking into account the condensation of other species, for
221 instance, amines and has been suggested to be a good quantitative representation
222 for the occurrence of NPF after comparing with L for NPF events observed at urban
223 Beijing (Deng et al., 2020). The detailed information to calculate I can be found in
224 (Cai et al., 2021a).

225 **3. Results and discussion**

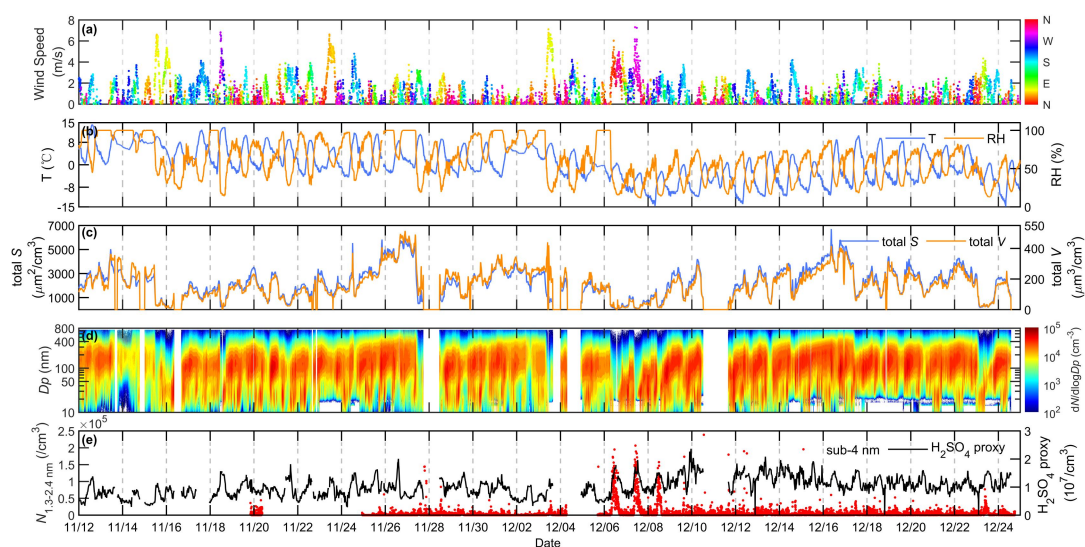
226 **3.1. General characteristics of NPF at GC site**

227 Figure 2 shows the time series of meteorological parameters (a: wind speed and
228 direction, b: temperature and relative humidity) and aerosol properties (c: total
229 surface and volume concentration, d and e: PNSD in the size range of 10 to 800 nm
230 and particle number concentration in the range of 1.3 to 2.4 nm) during this field
231 campaign. During our study, wind speed was typically quite low with an average of
232 $1.18 \text{ m}\cdot\text{s}^{-1}$, indicating stagnant meteorological conditions for the limited dilution of air
233 pollutants at the current site. The temperature and relative humidity (RH) show
234 opposite diurnal variation over the observational period, with the highest
235 temperature and lowest RH during daytime and vice versa during nighttime. The
236 observed time series of concentration of different trace gases during current study is
237 shown in Fig. S1. To be specific, the campaign-averaged concentration of CO, O₃, NO_x
238 and SO₂ was 1394 ppb, 7 ppb, 83 ppb and 10 ppb, respectively.

239 According to the PNSD and PSM data, five days, with four of which having
240 significant burst of sub-3 nm clusters as shown in Fig.2e, were classified as NPF
241 events out of the total experimental period. It has to be noted that on the day of
242 November 18, though PSM data was not available due to technical issues, clear
243 growth of nucleation mode particles with a typical banana-shape PNSD was observed,
244 lasting for more than 12 hours. These particles under the growth of such a long time
245 should not be from traffic emissions or transported. Therefore, it was also classified
246 as an event day in our study. Considering all these five NPF event, this corresponds
247 to an NPF frequency of 12.8%, which was lower than those at an urban site (i.e.,
248 Beijing) in the same region during the same season Shen et al. (2018) (25.8%); Deng
249 et al. (2020) (51.4%). Similar findings were also observed in Yue et al. (2009) and
250 Wang et al. (2013), that NPF frequencies were higher at the Beijing urban site than at
251 the corresponding regional background or rural site. Yue et al. (2009) and Wang et al.

252 (2013) attributed this to the higher pollution level and correspondingly higher
 253 precursor content in the urban cities, leading to stronger NPF events there.

254 During our study, six days, with a slightly weak burst of sub-3 nm particles, were
 255 identified as undefined days as their formation and growth rate cannot be calculated
 256 accurately. For non-event days, we observed that during many of them some
 257 nucleation-mode particles with size above 10 nm did appear. However, we did not
 258 observe the burst of sub-3 nm clusters from the PSM measurements and moreover
 259 no clear growth of these particles can be identified. This indicates that these small
 260 particles probably are not from nucleation of H₂SO₄ with other species and their
 261 subsequent growth, but more likely local emissions (traffic exhausts) or long-range
 262 transported.

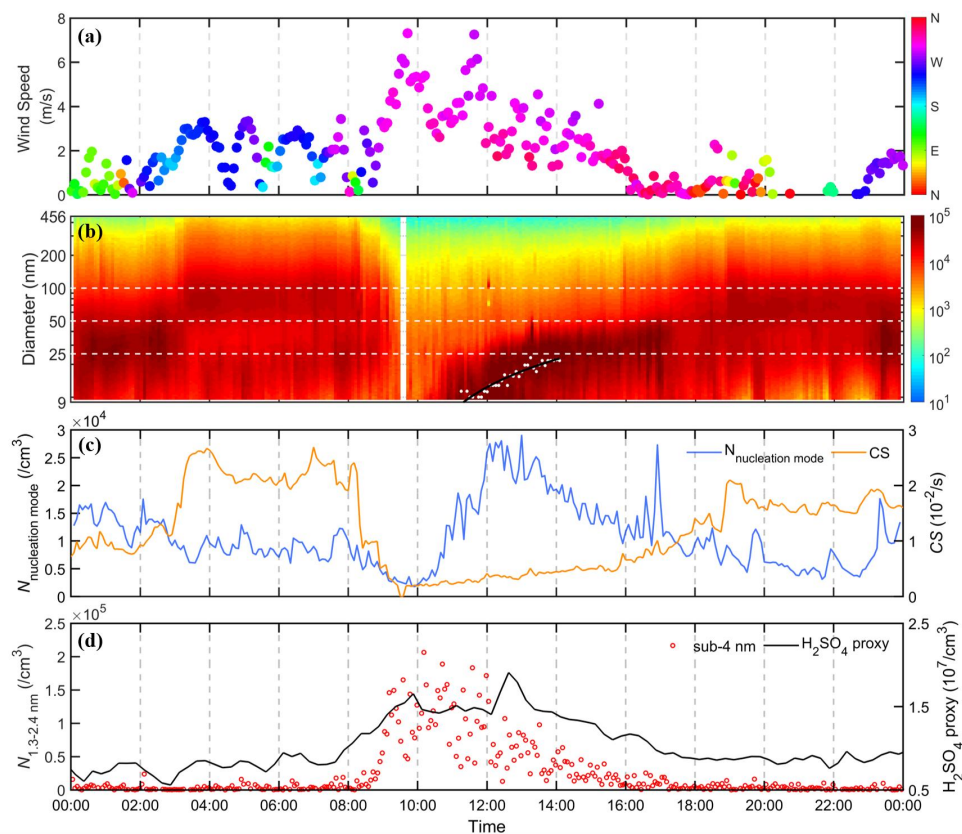


263
 264 **Figure 2.** Time series of (a) wind speed and wind direction, (b) temperature, (*T*) and relative
 265 humidity (RH), (c) total particle surface and volume concentration calculated by using PNSD data,
 266 (d) measured PNSD in the size range of 10 - 800 nm, (e) particle number concentration in the
 267 range of 1.3 to 2.4 nm and H₂SO₄ proxy concentration during the entire measurement period
 268 (2018.11.12-2018.12.24). White portion indicates no data was available due to instrument
 269 maintenance or power failure. Note that white portion in the PNSD in the size range of 10 - 15
 270 nm, indicating no available data, is due to the technical problems of our SMPS system; therefore
 271 data for that time period from a parallel SMPS covering sizes of 15 - 800 nm was used instead.

272

273 Figure 3 shows a typical NPF event on December 7 as an example. Northwest
 274 wind prevailed with elevated wind speed starting from around 8:00 o'clock, which
 275 was conducive to the diffusion of local pollutants, leading to a rapid decrease in CS

276 concurrently. At the same time, an obvious rise in H_2SO_4 concentration was observed,
 277 coinciding with a strong burst in the concentration of sub-3 nm clusters. Then, new
 278 particles with diameter larger than 10 nm, as shown in Fig. 3b, gradually formed by
 279 growth, exhibited as a visible banana shape in PNSD.



280 **Figure 3.** A case of NPF event on December 7 during this field campaign. Time series of (a) wind
 281 speed and wind directions, (b) the PNSD in the size range of 10 - 450 nm (The white dotted line
 282 represents the size with diameter at 25, 50, and 100 nm; black line represents the polynomial fit
 283 of the measured PNSD, (c) the particle number concentration of nucleation mode (9 - 25nm) and
 284 CS, (d) the number concentration of sub-3nm clusters and predicted concentration of sulfuric
 285 acid.
 286

287

288 For all the identified NPF events, the formation rate of 1.3 nm ($J_{1.3}$) particles
 289 ranged from $6.0 \text{ cm}^{-3}\cdot\text{s}^{-1}$ to about $30.4 \text{ cm}^{-3}\cdot\text{s}^{-1}$ with an average value of $22.0 \text{ cm}^{-3}\cdot\text{s}^{-1}$
 290 at our GC site during the measurement period. Note that most atmospheric
 291 formation rates reported in China were based on the measured formation rates at
 292 relatively larger size, i.e., 3-10 nm, which are so called the “apparent” particle
 293 formation rates. In order to derive the formation rates of critical clusters from the
 294 “apparent” particle formation rates (Kulmala et al., 2017), the nuclei GR or GR at

295 sub-3 nm is needed but usually remains unclear. Therefore, we focused more on the
296 formation rate of particles at sizes below 3 nm in the following discussion. In
297 principle, particle formation rate is inversely proportional to the CS, as the nucleation
298 precursors or clusters would be scavenged more rapidly under higher CS conditions,
299 leading to a slower nanoparticle formation with a lower J . However, as shown in
300 Table 1, in spite of the higher CS, the particle formation rates at our site appear to be
301 higher than those in clean environments. This kind of intensive NPF becomes more
302 noticeable for those Chinese megacities, such as Shanghai, Beijing and Nanjing,
303 having an even higher J and CS compared to that at our GC site. The most plausible
304 explanation could be the higher abundance of nucleating precursors for NPF in those
305 polluted atmospheres, which is indicated by the SA concentration, either measured
306 in urban Shanghai and Nanjing or calculated in our study. To be specific, the mean SA
307 proxy concentration during NPF at our GC site was around $1.4 \cdot 10^7 \text{ cm}^{-3}$, a factor of
308 around 30 higher than that at Hyytiälä in Finland (Nieminen et al., 2014). The SA
309 concentration during NPF at Shanghai (Xiao et al., 2015) and Nanjing (Herrmann et
310 al., 2014) was even higher, being around $4 \cdot 10^7 \text{ cm}^{-3}$.

311

312

313

314 **Table 1.** Summaries of the parameters (average value) relevant for NPF event during wintertime in
 315 China and other countries.

| Station | Period | Frequency | J ($\text{cm}^{-3}\cdot\text{s}^{-1}$) | GR ($\text{nm}\cdot\text{h}^{-1}$) | CS ($10^{-2}\cdot\text{s}^{-1}$) | SA ($10^6\cdot\text{cm}^{-3}$) | Reference |
|------------------------|--|-----------|--|---|---|---------------------------------------|----------------------------|
| GC ^R | 2018.11.18 | - | 3.15 (J_{10}) | 4.3 | 4.7 | 12.5 | This study |
| GC ^R | 2018.12.06 | - | 29.7 ($J_{1.3}$) | 1.8 | 0.7 | 14.4 | This study |
| GC ^R | 2018.12.07 | - | 30.4 ($J_{1.3}$) | 4.1 | 0.8 | 14.7 | This study |
| GC ^R | 2018.12.08 | - | 21.8 ($J_{1.3}$) | 8.1 | 2.7 | 13.5 | This study |
| GC ^R | 2018.12.23 | - | 6.0 ($J_{1.3}$) | 1.2 | 1.6 | 14.3 | This study |
| GC ^R (mean) | 2018.11.12-12.24 | 12.8% | 22.0 ($J_{1.3}$) | 3.9 | 2.1 | 13.9 | This study |
| Thissio ^{UB} | 2015.8-2016.8, 2017.2-2018.2 ^a | 10.3% | 1.55 (J_{10}) | 3.48 | 0.79 | 6.33 | (Kalkavouras et al., 2020) |
| New Delhi ^U | 2002.10.26-2002.11.9 | 53.3% | 7.3 (J_3) | 14.9 | 5.75 | - | (Mönkkönen et al., 2005) |
| Panyu ^U | Winter of 2011 | 21.3% | 0.89 (J_{10}) | 5.1 | 5.5 | - | (Tan et al., 2016) |
| Shanghai ^U | 2013.11.25-2014.1.25 | 21% | 188 ($J_{1.34}$) | 11.4 | 6.0 | 37 | (Xiao et al., 2015) |
| Nanjing ^U | 2011.11.18-2012.3.31 | 20% | 33.2 (J_2) | 8.5 | 2.4 | 45.3 | (Herrmann et al., 2014) |
| Hongkong ^U | 2010.10.25-2010.11.29 | 34.3% | 2.94($J_{5.5}$) | 3.86 | 0.8-6.2 | 9.17 | (Guo et al., 2012) |
| Beijing ^U | 2018.1.23-2018.3.31 | 51.5% | 38 ($J_{1.5}$) | 5.5 | 3.7 | 4.13 | (Chu et al., 2021) |
| Ziyang ^R | 2012.12.5-2013.1.5 | 23% | 5.2(J_3) | 3.6 | 7.4 | 6.7 | (Chen et al., 2014) |
| Melpitz ^R | Winter of 2003-2006 | 3% | 0.7 (J_3) | 5.6 | 1.2 | 0.123 | (Hamed et al., 2010) |
| Melpitz ^R | Winter of 1996-1997 | 10% | 4.9(J_3) | 4.1 | 0.9 | 0.259 | (Hamed et al., 2010) |
| Pingyuan ^R | 2017.11.3-2018.1.20 | 39.2% | 164.2 ($J_{1.6}$) | 3.9 | 1.9 | 2.45 | (Fang et al., 2020) |
| Xinken ^R | 2004.10.3-2004.11.5 | 25.9% | 0.5-5.4(J_3) | 2.2.-19.8 | - | - | (Liu et al., 2008) |
| Solapur ^R | 2018.10-2019.2 | 28.9% | 0.22-10.07(J_{15}) | 1.2-13.8 | 0.6-3 | - | (Varghese et al., 2020) |
| Cyprus ^{RB} | 2018.1-2018.2 | 69% | 16.4($J_{1.5}$) | 9.97 | 1.2 | - | (Baalbaki et al., 2020) |
| SEAS ^O | Winter of 2018 | 5% | 2.95(J_{10}) | 14.35 | 4.5 | - | (Kompalli et al., 2020) |
| SMEAR II ^B | Winter of 1996-2003 | 24.2% | 0.2-1.1(J_3) | 0.29-3.7 | 0.05-0.35 | 0.53 | (Dal Maso et al., 2005) |

316 SEAS: the southeastern Arabian Sea
317 R: rural site UB: urban background site RB: rural background site U: urban site. B: background site O: ocean
318 site
319 a: only in wintertime -: no number

320 Although the formation rate of 1.3 nm particles is relatively high, the
321 newly-formed particles at our GC site usually cannot grow into very large particles
322 within a short time, indicative by their low GR. The average value of $GR_{1.3-2.4}$ and
323 GR_{9-15} at our site was $0.5 \text{ nm}\cdot\text{h}^{-1}$ and $3.9 \text{ nm}\cdot\text{h}^{-1}$, respectively, being generally lower
324 than many clean environments (GR_{1-3} of $0.9 \text{ nm}\cdot\text{h}^{-1}$ for Hyytiälä (Kulmala, 2013), of
325 $5.1 \text{ nm}\cdot\text{h}^{-1}$ for Jungfrauoch (Boulon et al., 2010)), but similar to those at urban
326 Beijing (Chu et al., 2021) and rural Pingyuan (Fang et al., 2020). This could be
327 attributed by the high CS or CoagS at those polluted environments as the growth of
328 small particles is limited, which are more vulnerable to the coagulation scavenging.
329 However, despite the high CoagS, the observed GR at Shanghai and Nanjing was still
330 exceptionally high. This discrepancy suggests that besides the high concentration of
331 precursors, mainly H_2SO_4 , in polluted environments including both rural and urban
332 sites, other precursors with different efficiency for nanoparticle growth, and other
333 involving mechanisms, for instance, multiphase reactions, may all contribute to the
334 nanoparticle growth, yet to be elucidated.

335 **3.2. Potential mechanisms for NPF events in the rural NCP**

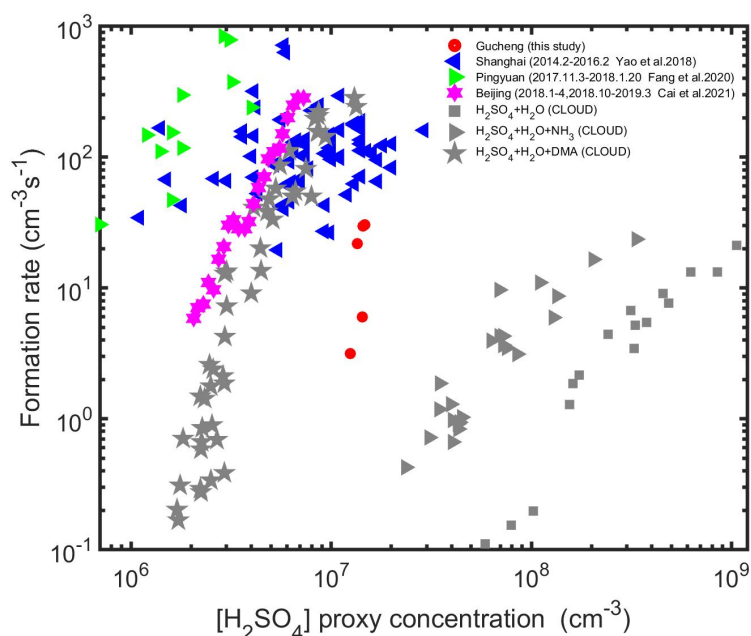
336 To further understand the dominating nucleation mechanism in the rural
337 atmosphere of NCP in China, we plotted the measured formation rate of 1.3 nm
338 particles ($J_{1.3}$) against the simulated H_2SO_4 concentration and compared the results
339 to previous studies conducted in different environments, as shown in Fig. 4. As
340 illustrated by the significant correlation between the concentration of sulfuric acid
341 and the particle formation rates, sulfuric acid is considered to be the driving species
342 in the initial steps of NPF as confirmed conventionally. However, the obtained
343 $J_{1.3}$ - H_2SO_4 relationship for current environment appeared to deviate largely from
344 those obtained by other studies. If only referring to the slope of the $J_{1.3}$ - H_2SO_4
345 relationship, our results seem to approximate most to the ones measured by these
346 CLOUD (The Cosmics Leaving OUtdoor Droplets chamber) experiments based on the
347 mechanism of H_2SO_4 -DMA nucleation. However, without the direct measurements of

348 other potential precursors, the molecules stabilizing H₂SO₄ clustering still remain
349 unclear.

350 Comparing the particle formation rates reported in different environments in
351 China, our results were of the similar magnitude as that in Beijing (Cai et al., 2021b),
352 an urban site in the NCP. It has to be noted that their study was conducted during a
353 much longer time and completely covered the measurement period of our study.
354 More importantly, during the five days of events in our study, NPF concurrently
355 occurred at their measurement site (Liu et al., 2020). Additionally, for these five
356 event days air masses arriving at our site followed similar transport paths to that at
357 urban Beijing (see Fig. S2 as an example in the supplement), both originating from
358 Siberia areas, where concentration of gaseous pollutants and particulate matter was
359 typically quite low, through the northwest of the observational sites. Taking both
360 evidence, we hypothesis that NPF events during these days in this area might be a
361 regional phenomenon, sharing the same or similar nucleation mechanism. Cai et al.
362 (2021) and Yan et al. (2021) further concluded that H₂SO₄-DMA was the dominating
363 nucleation mechanism for urban Beijing with an additional support from the
364 measured C2-amine concentration. Considering the similarities between these two
365 sites, we speculated that the clustering of H₂SO₄ with DMA may also dominate the
366 nucleation process at our site during winter, though future work is needed to verify
367 current hypothesis.

368 On the other hand, we noticed that our results deviate significantly from the
369 measured formation rate at Pingyuan (Fang et al., 2020), another rural site in the NCP.
370 They concluded that neither H₂SO₄-NH₃ nor H₂SO₄-DMA mechanisms could fully
371 explain their observed particle formation rate but suggested that gaseous
372 dicarboxylic acids were the dominating species for the initial step of H₂SO₄ clustering
373 under diacid-rich environment. Being likewise the rural environment of NCP, we
374 cannot completely rule out the contribution of dicarboxylic acids to the H₂SO₄
375 stabilizing. However, as illustrated in Fig. S4, the concentration of these four
376 dicarboxylic acids during NPF events were in general lower than that during
377 non-event days. Furthermore, during the daytime of events days when NPF was

378 typically initiated, the signals of these diacids obtained from the I-CIMS did not show
 379 clear increase, unlike sulfuric acid, but rather elevated during the night time (see Fig.
 380 S5), being obviously different from the case of Pingyuan. Hence, the involvements of
 381 diacids during the initial steps of nucleation under current rural atmosphere might
 382 not hold. This statement does not necessarily mean that our previous inference was
 383 incorrect, but on the other hand, provides some hints that though NPF events in the
 384 NCP is regional, there might be no uniform theory but multiple mechanisms
 385 coexisting to explain its feature with the dominating one varying upon different
 386 emission patterns or meteorological conditions.



387
 388 **Figure 4.** The particle formation rate ($J_{1,3}$) as a function of H_2SO_4 concentration for our study as
 389 well as for urban Shanghai (Yao et al., 2018), Beijing (Cai et al., 2021b), rural Pingyuan (Fang et al.,
 390 2020) and CLOUD measurements. Gray square, triangle, pentagram, and diamond represents the
 391 CLOUD data for $H_2SO_4+H_2O$, $H_2SO_4+H_2O+NH_3$, $H_2SO_4+H_2O+DMA$ (Kirkby et al. (2011) and
 392 Riccobono et al. (2014)), where DMA represents dimethylamine.

393

394 3.3 Governing factors for the occurrence of NPF in rural NCP

395

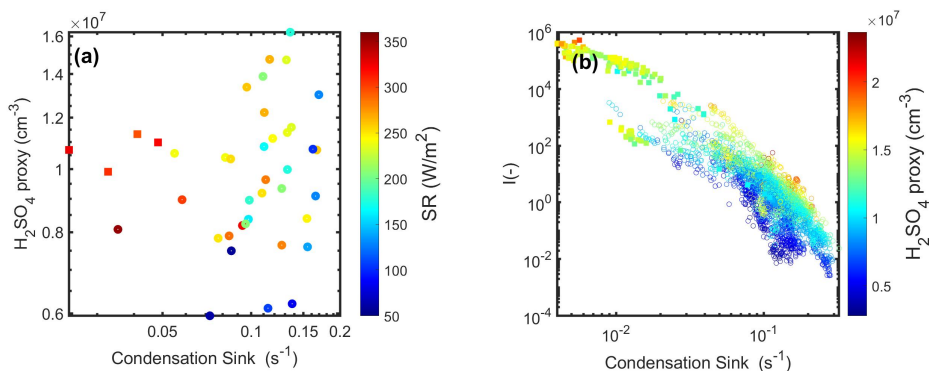
396 The high concentration of SO_2 , NH_3 , NO_x , VOCs (Chu et al., 2019) as well as fine
 397 particles makes the NCP of China an unique condition for NPF compared to many
 398 other environments. In principle, the competition between how fast the

399 newly-formed clusters grow and how fast they are scavenged determines whether
400 NPF will occur or not in the atmosphere. However, in the NCP, the concentration of
401 SA was typically quite high, probably reaching its maximum rate to form clusters.
402 Thus, CS or CoagS becomes the dominant factor controlling the occurrence of NPF.
403 This was partly confirmed by existing observations, for instance, Cai et al. (2021)
404 found that H₂SO₄ was high enough in urban Beijing, but not necessarily led to the
405 occurrence of NPF there. They pointed out that as long as CS or CoagS was below a
406 certain threshold (Cai et al., 2017), NPF is very likely take place.

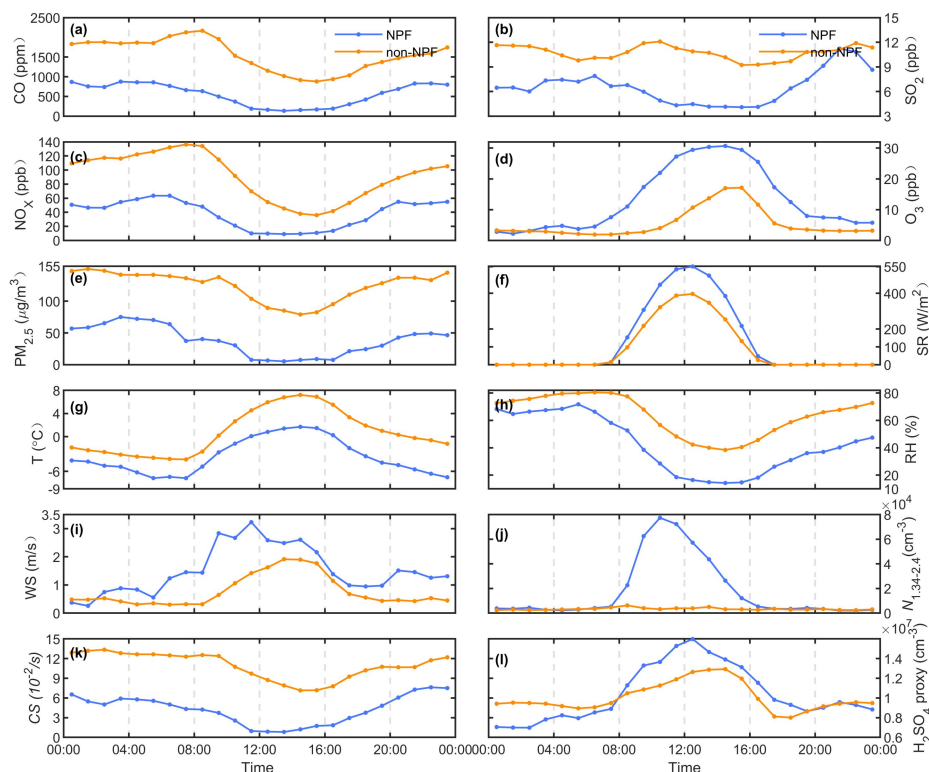
407 Was this also true for rural atmosphere in the NCP? By comparing with
408 non-event days at our site (see Fig. 5a), we noticed that H₂SO₄ level was not
409 significantly higher but sometimes even lower than that during non-event days. In
410 other words, the abundance of H₂SO₄ did not always lead to NPF; and it was only
411 when CS was significantly lowered that the event became more likely to occur. This
412 strongly demonstrates the similarity between our site with urban Beijing, that CS
413 would be the limiting factor for the occurrence of NPF. However, we noticed that
414 there were a very few cases (two cases) that CS was somewhat quite low, being
415 quite close to that under those event days, yet NPF still did not occur. The most
416 plausible explanation for this could be on the one hand the lowered H₂SO₄
417 concentration at these days (as shown in Fig. 5a) and on the other hand the other
418 nucleating species rather than H₂SO₄ may not be always enough to initiate
419 nucleation at this site.

420 As previously stated that the dimensionless criterion, *I*, is a good quantitative
421 indicator to predict whether an NPF occurs or not during a certain day, we plotted *I*
422 against the condensational sink for NPF days and other days under different H₂SO₄
423 level. Cai et al. (2021) found that the larger the *I* value, the higher frequency that
424 NPF events occurred for both urban Beijing and Shanghai, which was also clearly
425 revealed by our results. On the one hand, as shown in Fig. 5b, the largest *I* values
426 were mostly observed for NPF days, confirming its feasibility in predicting the
427 occurrence of NPF events. On the other hand, the obtained *I* anti-correlated with CS
428 quite well, while the influence from the available H₂SO₄ was not obvious. This

429 strongly suggests that CS was the dominating factor governing the appearance of
 430 NPF events at current environment, being highly consistent with the feature in
 431 Beijing.



432
 433 Figure 5. (a) H_2SO_4 concentration as a function of condensation sink during both event days
 434 (squares) and no-event days (circular dots) during our study. (b) The dimensionless indicator, I ,
 435 as a function of the condensational sink. The colorbar indicates: solar radiation (left panel) and
 436 H_2SO_4 proxy concentration (right panel).



437
 438 **Figure 6.** Diurnal variation of (a) CO, (b) SO_2 , (c) NO_x , (d) O_3 , (e) $PM_{2.5}$, (f) Solar radiation (SR), (g) T ,
 439 (h) RH, (i) wind speed (WS), (j) number concentration of sub-3nm cluster, (k) CS, and (l) H_2SO_4
 440 proxy during the NPF and non-NPF days during this field campaign. These values were
 441 averaged over the five NPF days and 28 non-event days, respectively.

442 On the other hand, we found that RH level under event days was generally
443 lower than that on non-event days (see Fig. 6). This is similar to the cases that NPF
444 was observed in Beijing by Yue et al. (2009), who suggested that photochemical
445 reactions were faster on sunny days with low RH. In addition to this, ambient
446 temperature during NPF was relatively lower than that on non-event days (Kirkby et
447 al. (2011); Riccobono et al. (2014)). Yan et al. (2021) considered that temperature can
448 affect the stability of H₂SO₄ clustering and thus influence NPF. Therefore, all these
449 factors could be the potential reasons increase or decrease the probability of NPF to
450 occur in current rural areas. It has to be noted that all these features, including
451 reduced RH level as well as ambient *T* during event days, could be coincidence with
452 reduced CS over clean days, for instance, being a consequence of air masses
453 originating from the north and bringing dryer, colder and cleaner air to the site.
454 Therefore, current discussion in this regard becomes ambiguous and may be inclusive,
455 but should still be considered separately when larger datasets are available.
456 Moreover, we observed that O₃ concentration was clearly higher during event days,
457 implying that other condensable vapors, for instance, organics, that involve O₃,
458 among others, in forming HOM, might also be important to NPF in this region.
459 Although these organic compounds formed through O₃ oxidation (Mohr et al., 2019)
460 may not necessarily participate in H₂SO₄ clustering, they may considerably contribute
461 to the growth of newly-formed particles, which should not be ruled out in the study
462 of NPF for this region and also need to be investigated in the future.

463

464 4. Summary and conclusions

465

466 Most previous studies dealing with NPF in China were mainly based on
467 measurements of particles at larger sizes, typically above 3 nm, whereas detection of
468 particles at sub-3 nm range was quite limited. In our study, by coupling a PSM with a
469 traditional SMPS, We were able to measure the particle number size distribution
470 down to 1.3 nm during NPF events in the wintertime at a rural site of the NCP.
471 Correspondingly, formation rate of particles at 1.3 nm was obtained, widening the

472 data pool concerning the feature of NPF for this region. At current rural environment,
473 high level of H_2SO_4 may not always initiate the occurrence of NPF. Only at the
474 condition that the CS was considerably low, NPF events were more likely to take place.
475 This feature is quite similar to that of the urban atmosphere of NCP, whereas NPF
476 events were usually characterized with high formation rates, high CS and high H_2SO_4
477 concentration. However, as our H_2SO_4 concentration was predicted from empirical
478 parameters, particular cautions regarding their associated uncertainties should be
479 considered. Yang et al. (2021) demonstrated that the derived fitting parameters for
480 the calculations of H_2SO_4 proxy may vary from site to site and between different
481 seasons. For instance, they considered the products from the ozonolysis of alkenes
482 were able to oxidize SO_2 to form gaseous H_2SO_4 . Moreover, they pointed out that
483 H_2SO_4 could be from primary emissions, such as vehicles or freshly emitted plumes.
484 Sulfuric acid from these sources could account for 10% of the total H_2SO_4 in the
485 atmosphere. These aspects were not comprehensively considered in our calculations,
486 which could bring huge uncertainties or errors to the estimation. Thereby, direct
487 measurements for the H_2SO_4 concentration should be implemented in the future
488 before driving any further conclusion.

489
490
491
492
493
494
495
496
497
498
499
500
501

502 **Declaration of interest statement.**

503 The authors declare that they have no known competing financial interests or
504 personal relationships that could have appeared to influence the work reported in
505 this paper.

506

507 **Data availability.**

508 The details data can be obtained from <https://doi.org/10.5281/zenodo.7326388>
509 (Hong, 2022).

510

511 **Author contributions.**

512 JH collected the resources, wrote and finalized the manuscript, MT analyzed the data,
513 plotted the figures and wrote the original draft, QQW and NM planned the study,
514 collected the resources, reviewed the manuscript. SWZ, SBZ, XHP, LHX, GL, UK
515 conducted the measurements, CY, JCT, YK, YH, YQZ, WYX, GSZ, BY, ZBW discussed the
516 results. YFC and HS contributed to fund acquisition.

517

518 **Competing interests.**

519 Hang Su and Yafang Cheng are members of the editorial board of Atmospheric
520 Chemistry and Physics

521

522 **Acknowledgements.**

523 This work is supported by the National Natural Science Foundation of China (grant no.
524 42175117, 41907182, 41877303, 91644218) and the National key R&D Program of
525 China (2018YFC0213901), the Fundamental Research Funds for the Central
526 Universities (21621105), the Guangdong Innovative and Entrepreneurial Research
527 Team Program (Research team on atmospheric environmental roles and effects of
528 carbonaceous species: 2016ZT06N263), and Special Fund Project for Science and
529 Technology Innovation Strategy of Guangdong Province (2019B121205004).

530 References

- 531 Almeida, J., Schobesberger, S., Kürten, A., Ortega, I. K., Kupiainen-Määttä, O., Praplan, A. P.,
532 Adamov, A., Amorim, A., Bianchi, F., Breitenlechner, M., David, A., Dommen, J., Donahue, N. M.,
533 Downard, A., Dunne, E., Duplissy, J., Ehrhart, S., Flagan, R. C., Franchin, A., Guida, R., Hakala, J.,
534 Hansel, A., Heinritzi, M., Henschel, H., Jokinen, T., Junninen, H., Kajos, M., Kangasluoma, J.,
535 Keskinen, H., Kupc, A., Kurtén, T., Kvashin, A. N., Laaksonen, A., Lehtipalo, K., Leiminger, M.,
536 Leppä, J., Loukonen, V., Makhmutov, V., Mathot, S., McGrath, M. J., Nieminen, T., Olenius, T.,
537 Onnela, A., Petäjä, T., Riccobono, F., Riipinen, I., Rissanen, M., Rondo, L., Ruuskanen, T., Santos, F.
538 D., Sarnela, N., Schallhart, S., Schnitzhofer, R., Seinfeld, J. H., Simon, M., Sipilä, M., Stozhkov, Y.,
539 Stratmann, F., Tomé, A., Tröstl, J., Tsagkogeorgas, G., Vaattovaara, P., Viisanen, Y., Virtanen, A.,
540 Vrtala, A., Wagner, P. E., Weingartner, E., Wex, H., Williamson, C., Wimmer, D., Ye, P., Yli-Juuti, T.,
541 Carslaw, K. S., Kulmala, M., Curtius, J., Baltensperger, U., Worsnop, D. R., Vehkamäki, H., and
542 Kirkby, J.: Molecular understanding of sulphuric acid-amine particle nucleation in the atmosphere,
543 *Nature*, 502, 359–363, <https://doi.org/10.1038/nature12663>, 2013.
- 544 Baalbaki, R., Pikridas, M., Jokinen, T., Laurila, T., Dada, L., Bezantakos, S., Ahonen, L., Neitola, K.,
545 Maisser, A., Bimenyimana, E., Christodoulou, A., Unga, F., Savvides, C., Lehtipalo, K.,
546 Kangasluoma, J., Biskos, G., Petäjä, T., Kerminen, V.-M., Sciare, J., and Kulmala, M.: Towards
547 understanding the mechanisms of new particle formation in the Eastern Mediterranean, *Atmos.*
548 *Chem. Phys. Discuss.*, 1–44, <https://doi.org/10.5194/acp-2020-1066>, 2020.
- 549 Berndt, T., Stratmann, F., Sipilä, M., Vanhanen, J., Petäjä, T., Mikkilä, J., Grüner, A., Spindler, G.,
550 Lee Mauldin, R., Curtius, J., Kulmala, M., and Heintzenberg, J.: Laboratory study on new particle
551 formation from the reaction OH + SO₂: Influence of experimental conditions, H₂O vapour, NH₃
552 and the amine tert-butylamine on the overall process, *Atmos. Chem. Phys.*, 10, 7101–7116,
553 <https://doi.org/10.5194/acp-10-7101-2010>, 2010.
- 554 Bianchi, F., Tröstl, J., Junninen, H., Frege, C., Henne, S., Hoyle, C. R., Molteni, U., Herrmann, E.,
555 Adamov, A., Bukowiecki, N., Chen, X., Duplissy, J., Gysel, M., Hutterli, M., Kangasluoma, J.,
556 Kontkanen, J., Kürten, A., Manninen, H. E., Münch, S., Peräkylä, O., Petäjä, T., Rondo, L.,
557 Williamson, C., Weingartner, E., Curtius, J., Worsnop, D. R., Kulmala, M., Dommen, J., and
558 Baltensperger, U.: New particle formation in the free troposphere: A question of chemistry and
559 timing, *Science (80-.)*, 352, 1109–1112, <https://doi.org/10.1126/science.aad5456>, 2016.
- 560 Boulon, J., Sellegri, K., Venzac, H., Picard, D., Weingartner, E., Wehrle, G., Collaud Coen, M.,
561 Bütikofer, R., Flückiger, E., Baltensperger, U., and Laj, P.: New particle formation and ultrafine
562 charged aerosol climatology at a high altitude site in the Alps (Jungfrauoch, 3580 m a.s.l.,
563 Switzerland), *Atmos. Chem. Phys.*, 10, 9333–9349, <https://doi.org/10.5194/acp-10-9333-2010>,
564 2010.
- 565 Cai, R. and Jiang, J.: A new balance formula to estimate new particle formation rate: Reevaluating
566 the effect of coagulation scavenging, *Atmos. Chem. Phys.*, 17, 12659–12675,
567 <https://doi.org/10.5194/acp-17-12659-2017>, 2017.
- 568 Cai, R., Yang, D., Fu, Y., Wang, X., Li, X., Ma, Y., Hao, J., Zheng, J., and Jiang, J.: Aerosol surface
569 area concentration: A governing factor in new particle formation in Beijing, *Atmos. Chem. Phys.*,
570 17, 12327–12340, <https://doi.org/10.5194/acp-17-12327-2017>, 2017.

571 Cai, R., Yan, C., Worsnop, D. R., Bianchi, F., Kerminen, V.-M., Liu, Y., Wang, L., Zheng, J., Kulmala,
572 M., and Jiang, J.: An indicator for sulfuric acid–amine nucleation in atmospheric environments,
573 *Aerosol Sci. Technol.*, 55, 1059–1069, <https://doi.org/10.1080/02786826.2021.1922598>, 2021a.

574 Cai, R., Yan, C., Yang, D., Yin, R., Lu, Y., Deng, C., Fu, Y., Ruan, J., Li, X., Kontkanen, J., Zhang, Q.,
575 Kangasluoma, J., Ma, Y., Hao, J., Worsnop, D. R., Bianchi, F., Paasonen, P., Kerminen, V. M., Liu, Y.,
576 Wang, L., Zheng, J., Kulmala, M., and Jiang, J.: Sulfuric acid-amine nucleation in urban Beijing,
577 *Atmos. Chem. Phys.*, 21, 2457–2468, <https://doi.org/10.5194/acp-21-2457-2021>, 2021b.

578 CHEN Chen, HU Min, WU Zhi-jun, WU Yu-sheng, GUO Song, CHEN Wen-tai, LUO Bin, SHAO Min,
579 ZHANG Yuan-hang, X. S.: Characterization of new particle formation event in the rural site of
580 Sichuan Basin and its contribution to cloud condensation nuclei., *China Environ. Sci.*, 34,
581 2764–2772, 2014.

582 Chu, B., Matti Kerminen, V., Bianchi, F., Yan, C., Petäjä, T., and Kulmala, M.: Atmospheric new
583 particle formation in China, *Atmos. Chem. Phys.*, 19, 115–138,
584 <https://doi.org/10.5194/acp-19-115-2019>, 2019.

585 Chu, B., Dada, L., Liu, Y., Yao, L., Wang, Y., Du, W., Cai, J., Dällenbach, K. R., Chen, X., Simonen, P.,
586 Zhou, Y., Deng, C., Fu, Y., Yin, R., Li, H., He, X. C., Feng, Z., Yan, C., Kangasluoma, J., Bianchi, F.,
587 Jiang, J., Kujansuu, J., Kerminen, V. M., Petäjä, T., He, H., and Kulmala, M.: Particle growth with
588 photochemical age from new particle formation to haze in the winter of Beijing, China, *Sci. Total*
589 *Environ.*, 753, 142207, <https://doi.org/10.1016/j.scitotenv.2020.142207>, 2021.

590 Dal Maso, M., Kulmala, M., Riipinen, I., Wagner, R., Hussein, T., Aalto, P. P., and Lehtinen, K. E. J.:
591 Formation and growth of fresh atmospheric aerosols: Eight years of aerosol size distribution data
592 from SMEAR II, Hyytiälä, Finland, *Boreal Environ. Res.*, 10, 323–336, 2005.

593 Deng, C., Fu, Y., Dada, L., Yan, C., Cai, R., Yang, D., Zhou, Y., Yin, R., Lu, Y., Li, X., Qiao, X., Fan, X.,
594 Nie, W., Kontkanen, J., Kangasluoma, J., Chu, B., Ding, A., Kerminen, V.-M., Paasonen, P.,
595 Worsnop, D. R., Bianchi, F., Liu, Y., Zheng, J., Wang, L., Kulmala, M., and Jiang, J.: Seasonal
596 Characteristics of New Particle Formation and Growth in Urban Beijing, *Environ. Sci. Technol.*,
597 [acs.est.0c00808](https://doi.org/10.1021/acs.est.0c00808), <https://doi.org/10.1021/acs.est.0c00808>, 2020.

598 Dunne, E. M., Gordon, H., Kürten, A., Almeida, J., Duplissy, J., Williamson, C., Ortega, I. K., Pringle,
599 K. J., Adamov, A., Baltensperger, U., Barmet, P., Benduhn, F., Bianchi, F., Breitenlechner, M.,
600 Clarke, A., Curtius, J., Dommen, J., Donahue, N. M., Ehrhart, S., Flagan, R. C., Franchin, A., Guida,
601 R., Hakala, J., Hansel, A., Heinritzi, M., Jokinen, T., Kangasluoma, J., Kirkby, J., Kulmala, M., Kupc,
602 A., Lawler, M. J., Lehtipalo, K., Makhmutov, V., Mann, G., Mathot, S., Merikanto, J., Miettinen, P.,
603 Nenes, A., Onnela, A., Rap, A., Reddington, C. L. S., Riccobono, F., Richards, N. A. D., Rissanen, M.
604 P., Rondo, L., Sarnela, N., Schobesberger, S., Sengupta, K., Simon, M., Sipilä, M., Smith, J. N.,
605 Stozkhov, Y., Tomé, A., Tröstl, J., Wagner, P. E., Wimmer, D., Winkler, P. M., Worsnop, D. R., and
606 Carslaw, K. S.: Global atmospheric particle formation from CERN CLOUD measurements, *Science*
607 (80-), 354, 1119–1124, <https://doi.org/10.1126/science.aaf2649>, 2016.

608 Ehn, M., Thornton, J. A., Kleist, E., Sipilä, M., Junninen, H., Pullinen, I., Springer, M., Rubach, F.,
609 Tillmann, R., Lee, B., Lopez-Hilfiker, F., Andres, S., Acir, I.-H., Rissanen, M., Jokinen, T.,
610 Schobesberger, S., Kangasluoma, J., Kontkanen, J., Nieminen, T., Kurtén, T., Nielsen, L. B.,
611 Jørgensen, S., Kjaergaard, H. G., Canagaratna, M., Maso, M. D., Berndt, T., Petäjä, T., Wahner, A.,
612 Kerminen, V.-M., Kulmala, M., Worsnop, D. R., Wildt, J., and Mentel, T. F.: A large source of
613 low-volatility secondary organic aerosol., *Nature*, 506, 476–9,
614 <https://doi.org/10.1038/nature13032>, 2014.

615 Fang, X., Hu, M., Shang, D., Tang, R., Shi, L., Olenius, T., Wang, Y., Wang, H., Zhang, Z., Chen, S.,
616 Yu, X., Zhu, W., Lou, S., Ma, Y., Li, X., Zeng, L., Wu, Z., Zheng, J., and Guo, S.: Observational
617 Evidence for the Involvement of Dicarboxylic Acids in Particle Nucleation, *Environ. Sci. Technol.*
618 *Lett.*, <https://doi.org/10.1021/acs.estlett.0c00270>, 2020.

619 Guo, H., Wang, D. W., Cheung, K., Ling, Z. H., Chan, C. K., and Yao, X. H.: Observation of aerosol
620 size distribution and new particle formation at a mountain site in subtropical Hong Kong, *Atmos.*
621 *Chem. Phys.*, **12**, 9923–9939, <https://doi.org/10.5194/acp-12-9923-2012>, 2012.

622 Guo, S., Hu, M., Zamora, M. L., Peng, J., Shang, D., Zheng, J., Du, Z., Wu, Z., Shao, M., Zeng, L.,
623 Molina, M. J., and Zhang, R.: Elucidating severe urban haze formation in China, *Proc. Natl. Acad.*
624 *Sci. U. S. A.*, **111**, 17373–17378, <https://doi.org/10.1073/pnas.1419604111>, 2014.

625 Hamed, A., Birmili, W., Joutsensaari, J., Mikkonen, S., Asmi, A., Wehner, B., Spindler, G., Jaatinen,
626 A., Wiedensohler, A., Korhonen, H., J. Lehtinen, K. E., and Laaksonen, A.: Changes in the
627 production rate of secondary aerosol particles in Central Europe in view of decreasing SO₂
628 emissions between 1996 and 2006, *Atmos. Chem. Phys.*, **10**, 1071–1091,
629 <https://doi.org/10.5194/acp-10-1071-2010>, 2010.

630 Herrmann, E., Ding, A. J., Kerminen, V. M., Petäjä, T., Yang, X. Q., Sun, J. N., Qi, X. M., Manninen,
631 H., Hakala, J., Nieminen, T., Aalto, P. P., Kulmala, M., and Fu, C. B.: Aerosols and nucleation in
632 eastern China: First insights from the new SORPES-NJU station, *Atmos. Chem. Phys.*, **14**,
633 2169–2183, <https://doi.org/10.5194/acp-14-2169-2014>, 2014.

634 Hussein, T., Dal Maso, M., Petäjä, T., Koponen, I. K., Paatero, P., Aalto, P. P., Hämeri, K., and
635 Kulmala, M.: Evaluation of an automatic algorithm for fitting the particle number size
636 distributions, *Boreal Environ. Res.*, **10**, 337–355, 2005.

637 Jokinen, T., Sipilä, M., Junninen, H., Ehn, M., Lönn, G., Hakala, J., Petäjä, T., Mauldin, R. L.,
638 Kulmala, M., and Worsnop, D. R.: Atmospheric sulphuric acid and neutral cluster measurements
639 using CI-API-TOF, *Atmos. Chem. Phys.*, **12**, 4117–4125,
640 <https://doi.org/10.5194/acp-12-4117-2012>, 2012.

641 Kalkavouras, P., Bougiatioti, A., Grivas, G., Stavroulas, I., Kalivitis, N., Liakakou, E., Gerasopoulos,
642 E., Pilinis, C., and Mihalopoulos, N.: On the regional aspects of new particle formation in the
643 Eastern Mediterranean: A comparative study between a background and an urban site based on
644 long term observations, *Atmos. Res.*, **239**, 104911,
645 <https://doi.org/10.1016/j.atmosres.2020.104911>, 2020.

646 Kirkby, J., Curtius, J., Almeida, J., Dunne, E., Duplissy, J., Ehrhart, S., Franchin, A., Gagné, S., Ickes,
647 L., Kürten, A., Kupc, A., Metzger, A., Riccobono, F., Rondo, L., Schobesberger, S., Tsagkogeorgas,
648 G., Wimmer, D., Amorim, A., Bianchi, F., Breitenlechner, M., David, A., Dommen, J., Downard, A.,
649 Ehn, M., Flagan, R. C., Haider, S., Hansel, A., Hauser, D., Jud, W., Junninen, H., Kreissl, F., Kvashin,
650 A., Laaksonen, A., Lehtipalo, K., Lima, J., Lovejoy, E. R., Makhmutov, V., Mathot, S., Mikkilä, J.,
651 Minginette, P., Mogo, S., Nieminen, T., Onnela, A., Pereira, P., Petäjä, T., Schnitzhofer, R.,
652 Seinfeld, J. H., Sipilä, M., Stozhkov, Y., Stratmann, F., Tomé, A., Vanhanen, J., Viisanen, Y., Vrtala,
653 A., Wagner, P. E., Walther, H., Weingartner, E., Wex, H., Winkler, P. M., Carslaw, K. S., Worsnop,
654 D. R., Baltensperger, U., and Kulmala, M.: Role of sulphuric acid, ammonia and galactic cosmic
655 rays in atmospheric aerosol nucleation, *Nature*, **476**, 429–435,
656 <https://doi.org/10.1038/nature10343>, 2011.

657 Kirkby, J., Duplissy, J., Sengupta, K., Frege, C., Gordon, H., Williamson, C., Heinritzi, M., Simon, M.,
658 Yan, C., Almeida, J., Trostl, J., Nieminen, T., Ortega, I. K., Wagner, R., Adamov, A., Amorim, A.,

659 Bernhammer, A. K., Bianchi, F., Breitenlechner, M., Brilke, S., Chen, X., Craven, J., Dias, A., Ehrhart,
660 S., Flagan, R. C., Franchin, A., Fuchs, C., Guida, R., Hakala, J., Hoyle, C. R., Jokinen, T., Junninen, H.,
661 Kangasluoma, J., Kim, J., Krapf, M., Kurten, A., Laaksonen, A., Lehtipalo, K., Makhmutov, V.,
662 Mathot, S., Molteni, U., Onnela, A., Perakyla, O., Piel, F., Petaja, T., Praplan, A. P., Pringle, K., Rap,
663 A., Richards, N. A. D., Riipinen, I., Rissanen, M. P., Rondo, L., Sarnela, N., Schobesberger, S., Scott,
664 C. E., Seinfeld, J. H., Sipila, M., Steiner, G., Stozhkov, Y., Stratmann, F., Tomé, A., Virtanen, A.,
665 Vogel, A. L., Wagner, A. C., Wagner, P. E., Weingartner, E., Wimmer, D., Winkler, P. M., Ye, P.,
666 Zhang, X., Hansel, A., Dommen, J., Donahue, N. M., Worsnop, D. R., Baltensperger, U., Kulmala,
667 M., Carslaw, K. S., and Curtius, J.: Ion-induced nucleation of pure biogenic particles, *Nature*, 533,
668 521–526, <https://doi.org/10.1038/nature17953>, 2016.

669 Kompalli, S. K., Nair, V. S., Jayachandran, V., Gogoi, M. M., and Babu, S. S.: Particle number size
670 distributions and new particle formation events over the northern Indian Ocean during
671 continental outflow, *Atmos. Environ.*, 238, 117719,
672 <https://doi.org/10.1016/j.atmosenv.2020.117719>, 2020.

673 Kuang, C., Riipinen, I., Sihto, S.-L., Kulmala, M., McCormick, A. V., and McMurry, P. H.: An
674 improved criterion for new particle formation in diverse atmospheric environments, *Atmos.*
675 *Chem. Phys.*, 10, 8469–8480, <https://doi.org/10.5194/acp-10-8469-2010>, 2010.

676 Kulmala, M.: Direct Observations of Atmospheric Aerosol Nucleation, *Science* (80-.), 943,
677 <https://doi.org/10.1126/science.1227385>, 2013.

678 Kulmala, M., Pirjola, L., and Mäkelä, J. M.: Stable sulphate clusters as a source of new
679 atmospheric particles, *Nature*, 404, 66–69, <https://doi.org/10.1038/35003550>, 2000.

680 Kulmala, M., Vehkamäki, H., Petäjä, T., Dal Maso, M., Lauri, A., Kerminen, V. M., Birmili, W., and
681 McMurry, P. H.: Formation and growth rates of ultrafine atmospheric particles: A review of
682 observations, *J. Aerosol Sci.*, 35, 143–176, <https://doi.org/10.1016/j.jaerosci.2003.10.003>, 2004.

683 Kulmala, M., Petäjä, T., Nieminen, T., Sipilä, M., Manninen, H. E., Lehtipalo, K., Dal Maso, M.,
684 Aalto, P. P., Junninen, H., Paasonen, P., Riipinen, I., Lehtinen, K. E. J., Laaksonen, A., and
685 Kerminen, V.-M.: Measurement of the nucleation of atmospheric aerosol particles, *Nat. Protoc.*,
686 7, 1651–1667, <https://doi.org/10.1038/nprot.2012.091>, 2012.

687 Kulmala, M., Petäjä, T., Ehn, M., Thornton, J., Sipilä, M., Worsnop, D. R., and Kerminen, V. M.:
688 Chemistry of atmospheric nucleation: On the recent advances on precursor characterization and
689 atmospheric cluster composition in connection with atmospheric new particle formation, *Annu.*
690 *Rev. Phys. Chem.*, 65, 21–37, <https://doi.org/10.1146/annurev-physchem-040412-110014>, 2014.

691 Kulmala, M., Kerminen, V.-M., Petäjä, T., Ding, A. J., and Wang, L.: Atmospheric gas-to-particle
692 conversion: why NPF events are observed in megacities?, *Faraday Discuss.*, 200, 271–288,
693 <https://doi.org/10.1039/C6FD00257A>, 2017.

694 Kulmala, M., Petäjä, T., Kerminen, V. M., Kujansuu, J., Ruuskanen, T., Ding, A., Nie, W., Hu, M.,
695 Wang, Z., Wu, Z., Wang, L., and Worsnop, D. R.: On secondary new particle formation in China,
696 *Front. Environ. Sci. Eng.*, 10, 1–10, <https://doi.org/10.1007/s11783-016-0850-1>, 2016.

697 Kürten, A., Bergen, A., Heinritzi, M., Leiminger, M., Lorenz, V., Piel, F., Simon, M., Sitals, R.,
698 Wagner, A. C., and Curtius, J.: Observation of new particle formation and measurement of
699 sulfuric acid, ammonia, amines and highly oxidized organic molecules at a rural site in central
700 Germany, *Atmos. Chem. Phys.*, 16, 12793–12813, <https://doi.org/10.5194/acp-16-12793-2016>,
701 2016.

702 Lin, W., Xu, X., Ge, B., and Zhang, X.: Characteristics of gaseous pollutants at Gucheng, a rural site

703 southwest of Beijing, *J. Geophys. Res. Atmos.*, 114, <https://doi.org/10.1029/2008JD010339>,
704 2009.

705 Liu, S., Hu, M., Wu, Z., Wehner, B., Wiedensohler, A., and Cheng, Y.: Aerosol number size
706 distribution and new particle formation at a rural/coastal site in Pearl River Delta (PRD) of China,
707 *Atmos. Environ.*, 42, 6275–6283, <https://doi.org/10.1016/j.atmosenv.2008.01.063>, 2008.

708 Liu, Y., Yan, C., Feng, Z., Zheng, F., Fan, X., Zhang, Y., Li, C., Zhou, Y., Lin, Z., Guo, Y., Zhang, Y., Ma,
709 L., Zhou, W., Liu, Z., Dada, L., Dällenbach, K., Kontkanen, J., Cai, R., Chan, T., Chu, B., Du, W., Yao,
710 L., Wang, Y., Cai, J., Kangasluoma, J., Kokkonen, T., Kujansuu, J., Rusanen, A., Deng, C., Fu, Y., Yin,
711 R., Li, X., Lu, Y., Liu, Y., Lian, C., Yang, D., Wang, W., Ge, M., Wang, Y., Worsnop, D. R., Junninen,
712 H., He, H., Kerminen, V. M., Zheng, J., Wang, L., Jiang, J., Petäjä, T., Bianchi, F., and Kulmala, M.:
713 Continuous and comprehensive atmospheric observations in Beijing: a station to understand the
714 complex urban atmospheric environment, *Big Earth Data*, 4, 295–321,
715 <https://doi.org/10.1080/20964471.2020.1798707>, 2020.

716 Lu, Y., Yan, C., Fu, Y., Chen, Y., Liu, Y., Yang, G., Wang, Y., Bianchi, F., Chu, B., Zhou, Y., Yin, R.,
717 Baalbaki, R., Garmash, O., Deng, C., Wang, W., Liu, Y., Petäjä, T., Kerminen, V. M., Jiang, J.,
718 Kulmala, M., and Wang, L.: A proxy for atmospheric daytime gaseous sulfuric acid concentration
719 in urban Beijing, *Atmos. Chem. Phys.*, 19, 1971–1983, <https://doi.org/10.5194/acp-19-1971-2019>,
720 2019.

721 Ma, N., Zhao, C., Tao, J., Wu, Z., Kecorius, S., Wang, Z., Groß, J., Liu, H., Bian, Y., Kuang, Y., Teich,
722 M., Spindler, G., Müller, K., Van Pinxteren, D., Herrmann, H., Hu, M., and Wiedensohler, A.:
723 Variation of CCN activity during new particle formation events in the North China Plain, *Atmos.*
724 *Chem. Phys.*, 16, 8593–8607, <https://doi.org/10.5194/acp-16-8593-2016>, 2016.

725 McMurry, P. H., Fink, M., Sakurai, H., Stolzenburg, M. R., Mauldin, I. L., Smith, J., Eisele, F., Moore,
726 K., Sjostedt, S., Tanner, D., Huey, L. G., Nowak, J. B., Edgerton, E., and Voisin, D.: A criterion for
727 new particle formation in the sulfur-rich Atlanta atmosphere, *J. Geophys. Res. Atmos.*, 110, 1–10,
728 <https://doi.org/10.1029/2005JD005901>, 2005.

729 Mikko Sipilä, Torsten Berndt, Tuukka Petäjä, David Brus, Joonas Vanhanen, Frank
730 Stratmann, Johanna Patokoski, Roy L. Mauldin III, Antti-Pekka Hyvärinen, Frank Stratmann,
731 Johanna Patokoski, Roy L. Mauldin III, Heikki Lihavainen, M. K.: The Role of Sulfuric Acid in
732 Atmospheric Nucleation, *Science* (80-.), 327, 1243–1246, 2010.

733 Mirme, S. and Mirme, A.: The mathematical principles and design of the NAIS - A spectrometer
734 for the measurement of cluster ion and nanometer aerosol size distributions, *Atmos. Meas. Tech.*,
735 6, 1061–1071, <https://doi.org/10.5194/amt-6-1061-2013>, 2013.

736 Mohr, C., Thornton, J. A., Heitto, A., Lopez-Hilfiker, F. D., Lutz, A., Riipinen, I., Hong, J., Donahue,
737 N. M., Hallquist, M., Petäjä, T., Kulmala, M., and Yli-Juuti, T.: Molecular identification of organic
738 vapors driving atmospheric nanoparticle growth, *Nat. Commun.*, 10, 4442,
739 <https://doi.org/10.1038/s41467-019-12473-2>, 2019.

740 Mönkkönen, P., Koponen, I. K., Lehtinen, K. E. J., Hämeri, K., Uma, R., and Kulmala, M.:
741 Measurements in a highly polluted Asian mega city: observations of aerosol number size
742 distribution, modal parameters and nucleation events, *Atmos. Chem. Phys. Discuss.*, 4,
743 5407–5431, <https://doi.org/10.5194/acpd-4-5407-2004>, 2005.

744 Nieminen, T., Lehtinen, K. E. J., and Kulmala, M.: Sub-10 nm particle growth by vapor
745 condensation-effects of vapor molecule size and particle thermal speed, *Atmos. Chem. Phys.*, 10,
746 9773–9779, <https://doi.org/10.5194/acp-10-9773-2010>, 2010.

747 Nieminen, T., Asmi, A., Aalto, P. P., Keronen, P., Petäjä, T., Kulmala, M., Kerminen, V. M.,
748 Nieminen, T., and Dal Maso, M.: Trends in atmospheric new-particle formation: 16 years of
749 observations in a boreal-forest environment, *Boreal Environ. Res.*, **19**, 191–214, 2014.

750 Petäjä, T., Mauldin, R. L., Kosciuch, E., McGrath, J., Nieminen, T., Paasonen, P., Boy, M., Adamov,
751 A., Kotiaho, T., and Kulmala, M.: Sulfuric acid and OH concentrations in a boreal forest site,
752 *Atmos. Chem. Phys.*, **9**, 7435–7448, <https://doi.org/10.5194/acp-9-7435-2009>, 2009.

753 Riccobono, F., Schobesberger, S., Scott, C. E., Dommen, J., Ortega, I. K., Rondo, L., Almeida, J.,
754 Amorim, A., Bianchi, F., Breitenlechner, M., David, A., Downard, A., Dunne, E. M., Duplissy, J.,
755 Ehrhart, S., Flagan, R. C., Franchin, A., Hansel, A., Junninen, H., Kajos, M., Keskinen, H., Kupc, A.,
756 Kürten, A., Kvashin, A. N., Laaksonen, A., Lehtipalo, K., Makhmutov, V., Mathot, S., Nieminen, T.,
757 Onnela, A., Petäjä, T., Praplan, A. P., Santos, F. D., Schallhart, S., Seinfeld, J. H., Sipilä, M.,
758 Spracklen, D. V., Stozhkov, Y., Stratmann, F., Tomé, A., Tsagkogeorgas, G., Vaattovaara, P.,
759 Viisanen, Y., Vrtala, A., Wagner, P. E., Weingartner, E., Wex, H., Wimmer, D., Carslaw, K. S.,
760 Curtius, J., Donahue, N. M., Kirkby, J., Kulmala, M., Worsnop, D. R., and Baltensperger, U.:
761 Oxidation products of biogenic emissions contribute to nucleation of atmospheric particles,
762 *Science (80-.)*, **344**, 717–721, <https://doi.org/10.1126/science.1243527>, 2014.

763 Shen, X., Sun, J., Zhang, X., Zhang, Y., Wang, Y., Tan, K., Wang, P., Zhang, L., Qi, X., Che, H., Zhang,
764 Z., Zhong, J., Zhao, H., and Ren, S.: Comparison of Submicron Particles at a Rural and an Urban
765 Site in the North China Plain during the December 2016 Heavy Pollution Episodes, *J. Meteorol.*
766 *Res.*, **32**, 26–37, <https://doi.org/10.1007/s13351-018-7060-7>, 2018a.

767 Shen, X., Sun, J., Kivekäs, N., Kristensson, A., Zhang, X., Zhang, Y., Zhang, L., Fan, R., Qi, X., Ma, Q.,
768 and Zhou, H.: Spatial distribution and occurrence probability of regional new particle formation
769 events in eastern China, *Atmos. Chem. Phys.*, **18**, 587–599,
770 <https://doi.org/10.5194/acp-18-587-2018>, 2018b.

771 Spracklen, D. V., Carslaw, K. S., Kulmala, M., Kerminen, V. M., Mann, G. W., and Sihto, S. L.: The
772 contribution of boundary layer nucleation events to total particle concentrations on regional and
773 global scales, *Atmos. Chem. Phys.*, **6**, 5631–5648, <https://doi.org/10.5194/acp-6-5631-2006>,
774 2006.

775 Stolzenburg, D., Simon, M., Ranjithkumar, A., Kürten, A., Lehtipalo, K., Gordon, H., Ehrhart, S.,
776 Finkenzeller, H., Pichelstorfer, L., Nieminen, T., He, X., Brilke, S., Xiao, M., Amorim, A., Baalbaki, R.,
777 Baccarini, A., and Beck, L.: Enhanced growth rate of atmospheric particles from sulfuric acid,
778 7359–7372, 2020.

779 Tan, H. B., Yin, Y., Li, F., Liu, X. T., Chan, P. W., Deng, T., Deng, X. J., Wan, Q. L., and Wu, D.:
780 Measurements of particle number size distributions and new particle formation events during
781 winter in the Pearl River Delta region, China, *J. Trop. Meteorol.*, **22**, 191–199,
782 <https://doi.org/10.16555/j.1006-8775.2016.02.009>, 2016.

783 Tröstl, J., Chuang, W. K., Gordon, H., Heinritzi, M., Yan, C., Molteni, U., Ahlm, L., Frege, C., Bianchi,
784 F., Wagner, R., Simon, M., Lehtipalo, K., Williamson, C., Craven, J. S., Duplissy, J., Adamov, A.,
785 Almeida, J., Bernhammer, A. K., Breitenlechner, M., Brilke, S., Dias, A., Ehrhart, S., Flagan, R. C.,
786 Franchin, A., Fuchs, C., Guida, R., Gysel, M., Hansel, A., Hoyle, C. R., Jokinen, T., Junninen, H.,
787 Kangasluoma, J., Keskinen, H., Kim, J., Krapf, M., Kürten, A., Laaksonen, A., Lawler, M., Leiminger,
788 M., Mathot, S., Möhler, O., Nieminen, T., Onnela, A., Petäjä, T., Piel, F. M., Miettinen, P., Rissanen,
789 M. P., Rondo, L., Sarnela, N., Schobesberger, S., Sengupta, K., Sipilä, M., Smith, J. N., Steiner, G.,
790 Tomè, A., Virtanen, A., Wagner, A. C., Weingartner, E., Wimmer, D., Winkler, P. M., Ye, P.,

791 Carslaw, K. S., Curtius, J., Dommen, J., Kirkby, J., Kulmala, M., Riipinen, I., Worsnop, D. R.,
792 Donahue, N. M., and Baltensperger, U.: The role of low-volatility organic compounds in initial
793 particle growth in the atmosphere, *Nature*, 533, 527–531, <https://doi.org/10.1038/nature18271>,
794 2016.

795 Vanhanen, J., Mikkilä, J., Lehtipalo, K., Sipil, M., Manninen, H. E., Siivola, E., and Petäjä, T.: Particle
796 Size Magnifier for Nano-CN Detection, *Aerosol Sci. Technol.*, 533–542,
797 <https://doi.org/10.1080/02786826.2010.547889>, 2011.

798 Varghese, M., Leena, P. P., Murugavel, P., Bankar, S., Todekar, K., Chowdhuri, S., Safai, P. D.,
799 Malap, N., Konwar, M., Dixit, S., Rao, Y. J., and Prabha, T. V.: New Particle Formation Observed
800 from a Rain Shadow Region of the Western Ghats India, *Toxicol. Environ. Chem.*, 0, 1–29,
801 <https://doi.org/10.1080/02772248.2020.1789134>, 2020.

802 Wang, Z., Wu, Z., Yue, D., Shang, D., Guo, S., Sun, J., Ding, A., Wang, L., Jiang, J., Guo, H., Gao, J.,
803 Cheung, H. C., Morawska, L., Keywood, M., and Hu, M.: New particle formation in China: Current
804 knowledge and further directions, *Sci. Total Environ.*, 577, 258–266,
805 <https://doi.org/10.1016/j.scitotenv.2016.10.177>, 2017.

806 Wang, Z. B., Hu, M., Sun, J. Y., Wu, Z. J., Yue, D. L., Shen, X. J., Zhang, Y. M., Pei, X. Y., Cheng, Y. F.,
807 and Wiedensohler, A.: Characteristics of regional new particle formation in urban and regional
808 background environments in the North China Plain, *Atmos. Chem. Phys.*, 13, 12495–12506,
809 <https://doi.org/10.5194/acp-13-12495-2013>, 2013.

810 Xiao, S., Wang, M. Y., Yao, L., Kulmala, M., Zhou, B., Yang, X., Chen, J. M., Wang, D. F., Fu, Q. Y.,
811 Worsnop, D. R., and Wang, L.: Strong atmospheric new particle formation in winter in urban
812 Shanghai, China, *Atmos. Chem. Phys.*, 15, 1769–1781, <https://doi.org/10.5194/acp-15-1769-2015>,
813 2015.

814 Yan, C., Yin, R., Lu, Y., Dada, L., Yang, D., Fu, Y., Kontkanen, J., Deng, C., Garmash, O., Ruan, J.,
815 Baalbaki, R., Schervish, M., Cai, R., Bloss, M., Chan, T., Chen, T., Chen, Q., Chen, X., Chen, Y., Chu,
816 B., Dällenbach, K., Foreback, B., He, X., Heikkinen, L., Jokinen, T., Junninen, H., Kangasluoma, J.,
817 Kokkonen, T., Kurppa, M., Lehtipalo, K., Li, H., Li, H., Li, X., Liu, Y., Ma, Q., Paasonen, P., Rantala, P.,
818 Pileci, R. E., Rusanen, A., Sarnela, N., Simonen, P., Wang, S., Wang, W., Wang, Y., Xue, M., Yang,
819 G., Yao, L., Zhou, Y., Kujansuu, J., Petäjä, T., Nie, W., Ma, Y., Ge, M., He, H., Donahue, N. M.,
820 Worsnop, D. R., Veli-Matti Kerminen, Wang, L., Liu, Y., Zheng, J., Kulmala, M., Jiang, J., and
821 Bianchi, F.: The Synergistic Role of Sulfuric Acid, Bases, and Oxidized Organics Governing
822 New-Particle Formation in Beijing, *Geophys. Res. Lett.*, 48, 1–12,
823 <https://doi.org/10.1029/2020GL091944>, 2021.

824 Yang, L., Nie, W., Liu, Y., Xu, Z., Xiao, M., Qi, X., Li, Y., Wang, R., Zou, J., Paasonen, P., Yan, C., Xu,
825 Z., Wang, J., Zhou, C., Yuan, J., Sun, J., Chi, X., Kerminen, V. M., Kulmala, M., and Ding, A.: Toward
826 Building a Physical Proxy for Gas-Phase Sulfuric Acid Concentration Based on Its Budget Analysis
827 in Polluted Yangtze River Delta, East China, *Environ. Sci. Technol.*, 55, 6665–6676,
828 <https://doi.org/10.1021/acs.est.1c00738>, 2021.

829 Yao, L., Garmash, O., Bianchi, F., Zheng, J., Yan, C., Paasonen, P., Sipilä, M., Wang, M., Wang, X.,
830 and Xiao, S.: Atmospheric new particle formation from sulfuric acid and amines in a Chinese
831 megacity, *Science (80-.)*, 281, 278–281, 2018.

832 Yu, H., Ren, L., and Kanawade, V. P.: New Particle Formation and Growth Mechanisms in Highly
833 Polluted Environments, *Curr. Pollut. Reports*, 3, 245–253,
834 <https://doi.org/10.1007/s40726-017-0067-3>, 2017.

835 Yue, D., Hu, M., Wu, Z., Wang, Z., Guo, S., Wehner, B., Nowak, A., Achtert, P., Wiedensohler, A.,
836 Jung, J., Kim, Y. J., and Liu, S.: Characteristics of aerosol size distributions and new particle
837 formation in the summer in Beijing, *J. Geophys. Res. Atmos.*, **114**, 1–13,
838 <https://doi.org/10.1029/2008JD010894>, 2009.

839 Zhang, R., Khalizov, A., Wang, L., Hu, M., and Xu, W.: Nucleation and Growth of Nanoparticles in
840 the Atmosphere, *Chem. Rev.*, **112**, 1957–2011, <https://doi.org/10.1021/cr2001756>, 2012.

841 Zhang, R., Wang, G., Guo, S., Zamora, M. L., Ying, Q., Lin, Y., Wang, W., Hu, M., and Wang, Y.:
842 Formation of Urban Fine Particulate Matter, *Chem. Rev.*, **115**, 3803–3855,
843 <https://doi.org/10.1021/acs.chemrev.5b00067>, 2015.

844 Zhang, Y., Tao, J., Ma, N., Kuang, Y., Wang, Z., Cheng, P., Xu, W., Yang, W., Zhang, S., Xiong, C.,
845 Dong, W., Xie, L., Sun, Y., Fu, P., Zhou, G., Cheng, Y., and Su, H.: Predicting cloud condensation
846 nuclei number concentration based on conventional measurements of aerosol properties in the
847 North China Plain, *Sci. Total Environ.*, **719**, 137473,
848 <https://doi.org/10.1016/j.scitotenv.2020.137473>, 2020.

849 Zhou, Y., Dada, L., Liu, Y., Fu, Y., Kangasluoma, J., Chan, T., Yan, C., Chu, B., Daellenbach, K. R.,
850 Bianchi, F., Kokkonen, T. V., Liu, Y., Kujansuu, J., Kerminen, V. M., Petäjä, T., Wang, L., Jiang, J.,
851 and Kulmala, M.: Variation of size-segregated particle number concentrations in wintertime
852 Beijing, *Atmos. Chem. Phys.*, **20**, 1201–1216, <https://doi.org/10.5194/acp-20-1201-2020>, 2020.

853